Organic Electronics 61 (2018) 276–281

Contents lists available at ScienceDirect

Organic Electronics

journal homepage: www.elsevier.com/locate/orgel

Impedance spectroscopy and capacitance – voltage measurements analysis: Impact of charge carrier lifetimes and mapping vertical segregation in bulk heterojunction P3HT: PCBM solar cells

O. Oklobia[a], S. Komilian[b], T. Sadat-Shafai[b,*]

[a] Centre for Solar Energy Research, College of Engineering, Swansea University, OpTIC Centre St. Asaph Business Park, LL17 0JD, UK
[b] Thin Film Laboratory, School of Engineering & Creative Arts, Staffordshire University, Sciences Centre, Leek Road, Stoke-on-Trent, ST4 2DF, UK

ARTICLE INFO

Keywords:
Characterisation
Impedance spectroscopy
Capacitance
Voltage
Flat band potential
Charge Carrier lifetime
Vertical segregation

ABSTRACT

Impedance spectroscopy measurement is employed to study the impact of thermal annealing on charge carrier lifetimes in P3HT: PCBM bulk heterojunction solar cells. Upon thermal annealing at 150 °C, a correlation between charge carrier lifetime and device performance is identified. The best power conversion efficiency reported here corresponds to the devices annealed at 150 °C, yielding the longest charge carrier life time. In addition to lateral segregation, thermal annealing promotes accumulation of PCBM molecular aggregates towards the cathode inducing vertical segregation as is evident from the analysis of results obtained from capacitance – voltage measurements. Based on Mott-Schottky relation, the measured values of the flat band potential as a function of thermal annealing is correlated to the concentration of PCBM at cathode interface and a compositional gradient profile induced by thermal annealing is proposed.

1. Introduction

Applications of solution – processable organic semiconductors in optoelectronic devices have become increasingly popular in the past few years [1,2]. This has been driven by their potential for fabricating highly efficient devices; owing to their ease of synthesis, tuneable optical and electronic properties, low cost fabrication and flexibility of their devices [3–5]. Amongst the various organic semiconductors, the use of composite polymers and fullerenes for organic solar cells (OSCs) have received extensive interests within the academia and industry [6,7]. OSCs fabricated from the blend of polymer, poly (3-hexylthiophene) (P3HT) and fullerene [6,6],-phenyl-C_{61}-butyric acid methyl ester (PCBM) have been the subject of much investigations over the past decade [8–11]. The structure and morphology of bulk heterojunction (BHJ) active layers of these devices are critical to their power conversion efficiencies (PCEs) [12–14]. These have a significant impact on operational parameters, such as exciton dissociation [15]; charge generation and transport [16] and subsequently the PCE of the completed device. For P3HT: PCBM – based solar cells, thermal annealing has been proven as one of the most effective method for tuning active layer morphologies [17]. In our previous studies, by gradually annealing to about 150 °C, best PCE for devices fabricated from 1:1 blends of P3HT: PCBM was obtained [13]. A combination of UV–Vis absorption spectroscopy and optical microscopy was employed to elucidate the association of the fullerene molecular segregation and D/A phase separation within the photoactive bulk; establishing a correlation between morphological variation and device performance. Other reported experimental techniques include Photoluminescence (PL) spectroscopy in probing charge transfer dynamics [19]; grazing incidence X-ray diffraction studies in providing insight into molecular conformations [18,20]. Combined with direct current (dc)–voltage characterisations, these methods have been frequently applied for evaluating PCEs of polymer/fullerene BHJ solar cells. Although widely used, dc measurements are informative at best and can provide useful insight in device parameters such as series resistance [21]. They are often presented to a degree, as an indirect assessment of the charge carrier mobility (properties) within the bulk and charge collection at the interface [21,22]. Alternatively, alternating current (ac) measurements due to their voltage dependence on frequency, can be directly applied to probe the electrical properties of both bulk and interfaces [23]. AC impedance spectroscopy (IS) measurements is a very useful method, in providing relevant insights into the mechanisms of devices such as the dye sensitized solar cell (DSSC) [24–26], organic field-effect transistors (OFETs) [27], and organic light emitting diodes (OLEDs) [28]. Compared to dc measurements, the application of IS measurements in OSCs is relatively limited. Even so, some of the reports on this method have

* Corresponding author.
E-mail address: t.sadat-shafai@staffs.ac.uk (T. Sadat-Shafai).

https://doi.org/10.1016/j.orgel.2018.06.003
Received 21 February 2018; Received in revised form 24 May 2018; Accepted 5 June 2018
Available online 06 June 2018

provided interesting information on charge carrier mobility and lifetimes in the devices' active layer [29–31]. Previously, we investigated the impact of charge carrier mobility on recombination mechanisms in the P3HT: PCBM based solar cells [32]. Depending on processing conditions, phase separation in the active layer influences the respective charge carrier mobilities. Optimum annealing highlighted a relatively prominent trap-assisted recombination mechanism (above its Langevin counterpart), largely attributable to PCBM molecular segregation.

In the present study, we investigate the significance of charge carrier lifetimes to device efficiencies and its impact on recombination employing ac analysis. Unlike dc methods, it is possible to elucidate the role of interfaces within the bulk active layer of OSCs directly [33]. From the analysis of impedance responses of devices under varying illumination intensities and bias conditions, as a function of thermal annealing conditions, we are able to highlight the significance of charge carrier lifetimes to device performance. In addition to IS measurements, capacitance–voltage (*C-V*) characterisation technique for mapping thermal annealing induced vertical segregation in polymer/fullerene BHJ solar cells is presented.

2. Experimental

P3HT (regioregularity of 96.6%, Ossila Ltd.), and PCBM (Solenne BV, The Netherlands), were used as purchased. A 1:1 blend of P3HT: PCBM, with a concentration of 25 mg/ml in dichlorobenzene (DCB), was used in this study. Details of the blend preparation procedure, device fabrication and current–voltage characterisation under illumination can be found elsewhere [13]. The structure of the devices fabricated is ITO/PEDOT: PSS/P3HT: PCBM/Al. The active layer thickness of the device is ~150 nm. Both IS and *C-V* measurements were performed using a HP 4284 A LCR Precision meter. The complex ac impedance spectra were measured in *Z–θ* mode, for a frequency range of 20 Hz to 1 MHz. The oscillating amplitude was between 20 and 50 mV, with an applied dc bias of 0.5 V. For the *C-V* measurements, a fixed frequency of 1 kHz was used, with an ac voltage of 0.05 V. A LABVIEW programme, controlling the LCR meter via a GPIB interface was used to acquire all IS and *C-V* data. All IS data obtained were fitted to appropriate equivalent circuits, using an EIS Spectrum Analyzer software [34].

3. Results and discussions

3.1. Current density – voltage (J – V) characteristics

The *J–V* characteristics of P3HT: PCBM devices are shown in Fig. 1 and extracted parameters are presented in Table 1. The devices were thermally annealed at 50, 75, 100, 125, 150 and 175 °C, for 10 min each. It is evident from Table 1, that the short circuit current density J_{SC} improves with annealing temperature up to around 150 °C after which deterioration in J_{SC} is observed. In contrast, the open circuit voltage, V_{OC} tends to reduce upon thermal annealing up to 100 °C, there after it increases with further thermal annealing. In all cases the power conversion efficiencies tend to follow the same trend as J_{SC}, with the highest PCE recorded at 150 °C. A possible reason for the observed J_{SC} dependence on thermal annealing could be improved polymer crystallinity, and favourable D/A separation. Improved crystallinity in the donor phase would ensure efficient exciton generation [15]. Other contributory factors include efficient exciton dissociation, improved charge carrier mobilities and the transport of charges to the respective electrodes [16,19]. The impact of these factors has been carefully studied and discussed previously [32]. However, in this paper, we focus on the impact of charge carrier lifetimes. According to the Braun's model on Photogeneration, charge transfer states have a finite lifetime [35] and once separated, they can again form a bound pair. The reformed and long-lived charge transfer states subsequently act as a precursor for free charge carriers [36]. We believe the longevity of charge carriers, along with optimised D/A phase separations, ensures efficient charge collection.

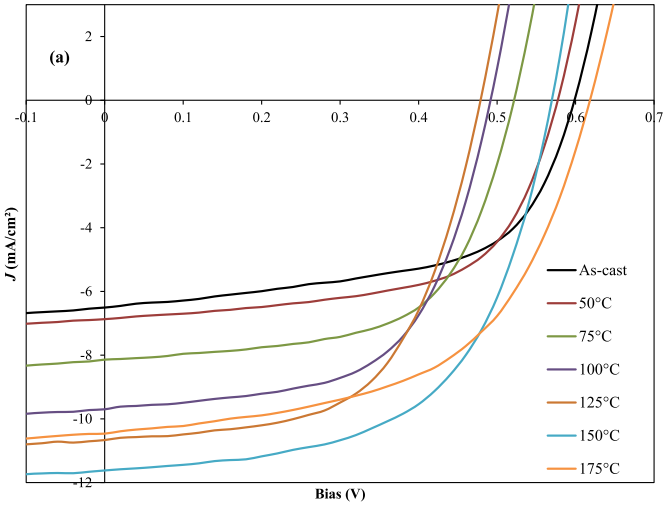

Fig. 1. *J – V* characteristics of BHJ P3HT: PCBM – based devices of as cast and after thermal annealing from 50 to 175 °C (in steps of 25 °C, 10 min).

Table 1
Summary of PV parameters: Short circuit current densities (J_{SC}), open circuit voltage (V_{OC}), fill factor (*FF*), power conversion efficiency (PCE).

	J_{sc} (mA/cm^2)	V_{oc} (V)	*FF*	PCE (%)
As-cast	6.51	0.60	0.58	2.26
50 °C	6.87	0.58	0.61	2.42
75 °C	8.14	0.52	0.61	2.60
100 °C	9.70	0.49	0.60	2.84
125 °C	10.67	0.48	0.59	3.00
150 °C	11.62	0.57	0.58	3.84
175 °C	10.46	0.62	0.55	3.56

3.2. Impedance spectroscopy measurements

The impedance measurements for our BHJ devices with the structure ITO/PEDOT: PSS/P3HT: PCBM/Al are presented using Cole-Cole plots in Fig. 2. In the low frequency IS response of the device (as cast) under 1 sun illumination and short circuit condition, we note that the resistance (x-intercept) approaches the shunt resistance extracted from the *J–V* curve under similar conditions (~2500 Ω). This observation is consistent with previous work by Leever et al. [33], supporting the correlation between impedance response and the device *I-V* curve. To extract further information associated with our device's electrical response, we fitted the impedance data to an equivalent circuit model. As is evident, the impedance spectra (Figs. 2 and 4) does not exhibit very smooth semi-circular arcs, indicating more than one pair of resistance–capacitance (in parallel) in an equivalent circuit [37], was required to provide a fit. This contrasts with a single semi-circular arc that have been shown to be well fitted to an equivalent circuit consisting of a resistor in series with a parallel resistance-capacitance combination [33]. The equivalent circuit model described by Yoon et al. [38], shown in Fig. 3, gave a good quality fit to our impedance responses as depicted in Figs. 2 and 4. R_S corresponds to the Re Z axis intercept at high frequencies. This resistance accounts for the resistive losses at the ITO/PEDOT: PSS interface [33,38], which almost remains constant under varied illumination and sample bias (Fig. 2). The $R_2||$CPE combination, where CPE is a constant phase element with an equivalent capacitance C_{eq} corresponds to a recombination resistance and chemical capacitance respectively. Both R_2 and CPE are generally accepted to be associated with charge transfer processes at D/A

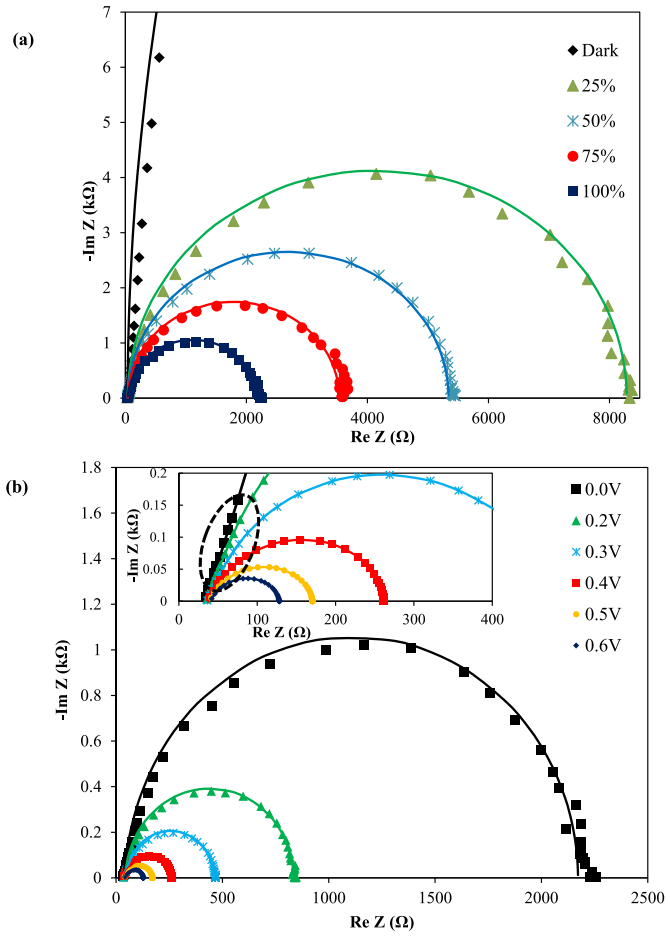

Fig. 2. Impedance spectra of P3HT: PCBM (1:1) solar cell (as cast): (a) at 0.0 V and under varied illumination intensities, (b) under 1 sun (100%) illumination intensity and varied bias.

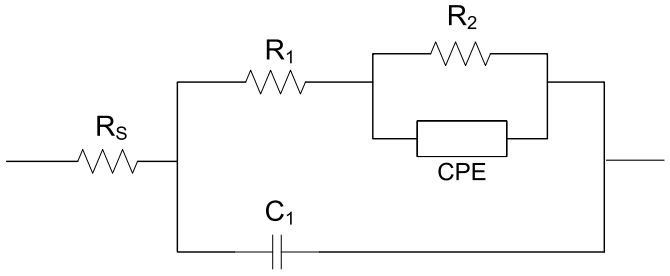

Fig. 3. Equivalent circuit representing P3HT: PCBM BHJ solar cell.

interfaces [33,38], and $R_1||C_1$ associated with the bulk resistance (in parallel with the external interface) and capacitance [23,38].

Impedance responses of our P3HT: PCBM–based devices as a function of thermal annealing temperatures are shown in Fig. 4 (a). The parameters R_1, R_2, C_1, and C_{eq} were extracted from the fitting of the equivalent circuit model in Fig. 3, where the average charge carrier lifetime (τ_{avg}) was calculated using the following equation:

$$\tau_{avg} = R_2 C_{eq} \quad (1)$$

and are summarised in Table 2 Although the equivalent circuit model employed in this work provided a good fit to the impedance data, we also examined an alternative model [39,40]. We found that in comparison to the model in Fig. 2, the alternative equivalent circuit model did not provide a fit of the data in this work, as can be seen depicted in Fig. 4(b). A correlation between thermal annealing and charge carrier

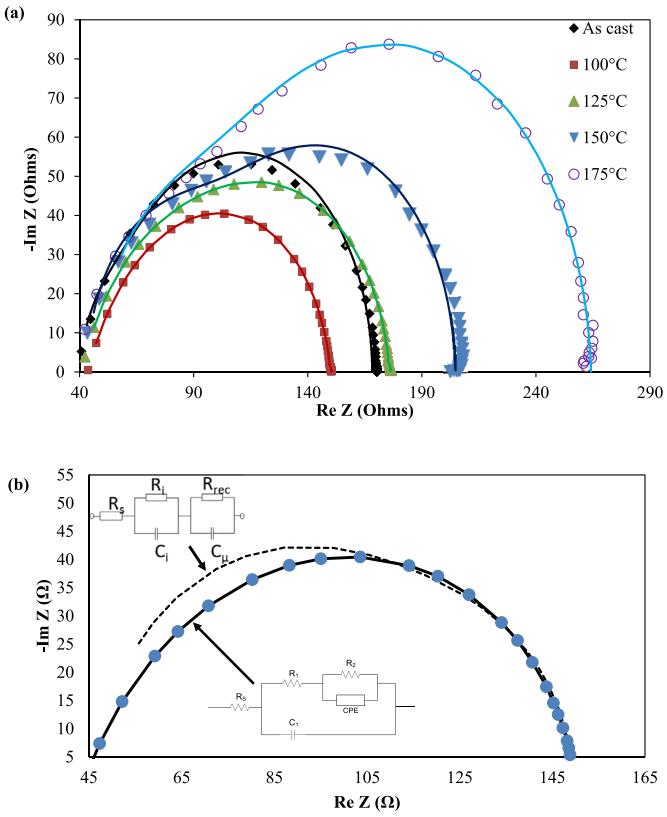

Fig. 4. (a) Impedance response of P3HT: PCBM solar cell; as cast and thermally annealed at various temperatures, at a sample bias of 0.5 V (i.e., around *Voc*) and under 1 sun illumination. The solid lines represent the fits to equivalent circuit model, (b) Comparison between equivalent circuit model fittings to experimental impedance data.

Table 2
A summary of the equivalent circuit parameters, extracted from the model fit to ac IS response experimental data.

1 sun (at 0.5 V)	R_1 (Ω)	R_2 (Ω)	C_1(F)	C_{eq}(F)
As cast	56.532	71.132	1.25×10^{-8}	3.54×10^{-8}
100 °C	51.87	48.041	1.22×10^{-8}	6.10×10^{-8}
125 °C	67.87	60.041	1.18×10^{-8}	7.10×10^{-8}
150 °C	85.88	75.200	1.01×10^{-8}	8.29×10^{-8}
175 °C	96.94	118.740	4.65×10^{-9}	3.56×10^{-8}

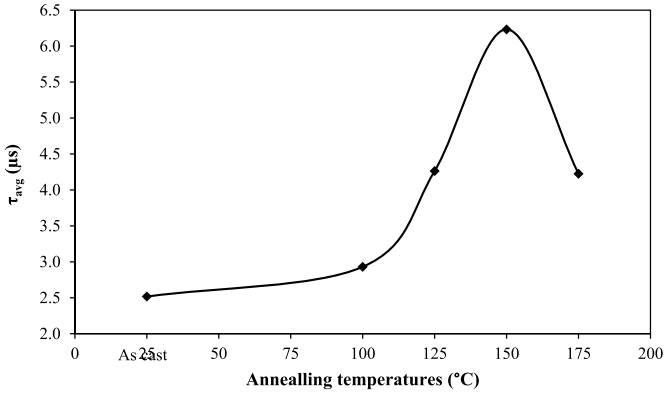

Fig. 5. A plot of carrier lifetimes as a function of thermal annealing temperatures.

lifetimes was confirmed, as shown in Fig. 5. As the annealing temperature was increased from 50 to 100 °C, a slight improvement in τ_{avg} was observed. Further thermal annealing beyond 100 °C resulted in a significant rise in the average carrier lifetime, with maximum value recorded after annealing at 150 °C (6.23 μs). Beyond this temperature, it was observed that τ_{avg} abruptly deteriorates. It should be noted however, that the range of carrier lifetimes (2.52–6.23 μs) determined here, is typical of P3HT:PCBM systems, and are in agreement with previous reports [33,38,41]. Furthermore, the charge carrier densities of the devices were calculated by integration of the chemical capacitance (C_{eq}) at the applied voltage (0.5 V) near V_{OC} [42]. These were found to be in the range of 10^{16}–10^{17} cm^{-3}, consistent with other reports [41,42]. Our best device efficiency obtained after annealing at 150 °C, could presumably be due to the longer average carrier lifetime that contributed to an improved charge collection, leading to higher current density values, as shown in Table 1. This strongly suggests that the thermal annealing of devices at around 150 °C induced phase segregations with optimised D/A interfaces and efficient bulk transport networks. Our previous study on similar device indicated an increase in decay rate constant associated with germinate recombination upon thermal annealing at 150 °C [32]. It was concluded that an increase in hole carrier mobility could have been responsible for improved PCE resulting from thermal annealing at 150 °C. Additionally, we also suspect in the present study, that the increase in charge carrier lifetimes could also be due to the reformation of interfacial charge–transfer states [16], as it is a possibility that should be completely ruled out.

Vertical segregation of the composite P3HT and PCBM blends have been previously observed [14,42]. This has mostly been attributed to their different solubilities, surface energies and the dynamics during spin casting processes [43,44]. Although lateral phase separation is induced by thermal annealing, it is also believed that the same process could lead to vertical segregation [14]. To verify the impact of thermal annealing on vertical segregation we have employed *C–V* measurement technique, which is discussed further in the following section.

3.3. Capacitance – Voltage (C – V) measurement analysis

The nature of interfacial interaction between the back electrode and P3HT: PCBM blend using a *C–V* measurement analysis, was previously reported by Guerrero et al. [45]. In their work they demonstrated the significance of charge-neutrality layer (CNL) [46] to metal/organic contact equilibration, highlighting the separate contributions from the bulk band bending and that from the interfacial dipole layer. Considering these factors, the cathode equilibration has been expressed in terms of the energy (qV_{fb}) required to overcome active layer band bending leading to flat-band condition according to the relation [47].

$$qV_{fb} = E_F - \phi_C - \Delta \quad (2)$$

Where V_{fb} is the potential under flat-band condition at the cathode, E_F the active layer Fermi level, ϕ_C is the cathode Fermi level and Δ the interfacial dipole formed at the active layer/cathode interface. For a given polymer/fullerene system V_{fb} is largely dependent on the magnitude of Δ, which have been demonstrated to be sensitive to the amount of fullerene formed at the interface [46,47]. By performing a Mott-Schottky analysis, the degree of fullerene coverage (or concentration) on or towards the film surface of active layers polymer/fullerene blends can therefore be probed. The accumulation of a particular specie of the composite blend (either electron donor or acceptor material) plays a significant role in carrier selectivity at respective electrodes [47]. The Mott – Schottky relation is given as $C^{-2} = 2(V_{fb} - V)/A^2 q\varepsilon_r\varepsilon_0 N$, where N is defined as the concentration of acceptor impurities, V applied voltage, A device active area (0.13 cm^2 in this work), q the electronic charge, and ε_r the relative dielectric constant, ε_0 permittivity of vacuum.

Our experimental *C–V* data was found to follow the C^{-2} vs. V Mott – Schottky characteristics, shown in Fig. 6, for our P3HT: PCBM blend devices: as cast and after annealing at 150 °C. It exhibits a straight line over a wide bias voltage range, from which V_{fb} and N, for as cast and thermally annealed devices were extracted, (assuming ε_r is 3.4 for P3HT: PCBM). These are summarised in Table 3.

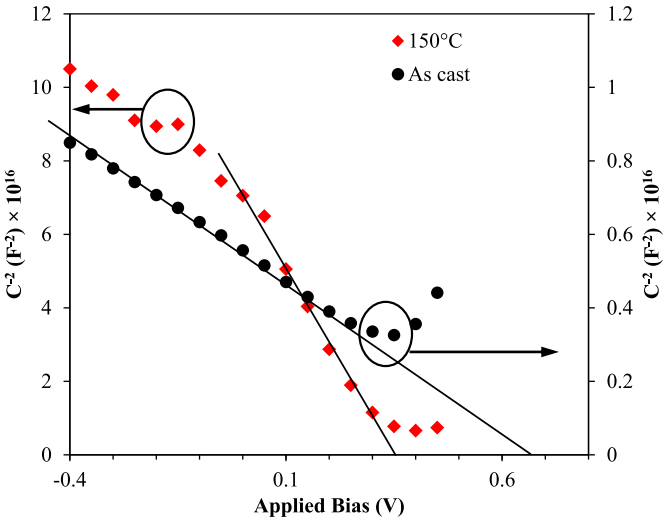

Fig. 6. Mott-Schottky curve of ITO/PEDOT: PSS/P3HT: PCBM/Al device; as cast and after thermal annealing at 150 °C.

Table 3
Summary of parameters extracted from Mott-Schottky curve.

	V_{fb}(V)	N (cm^{-3})
As cast	0.68	4.15×10^{17}
100 °C	0.50	5.93×10^{16}
125 °C	0.39	2.08×10^{16}
150 °C	0.34	1.38×10^{16}
175 °C	0.35	1.04×10^{16}

The values of N estimated in the present work are within the range of reported values in literature [48,49]. Extracted values of V_{fb} reveal an interesting correlation with thermal annealing. A flat band potential of 0.68 V was determined for as cast device, which is consistent with reported values [47]. Although V_{fb} values above 0.68 V have been previously reported [47] for a P3HT: PCBM system, it is important to mention that the difference in processing conditions could account for such variation in flat band potentials. As such fullerene distribution at the active layer/cathode interface is expected to differ, according to the interfacial dipole strength (see Eq. (2)). Upon thermal annealing (100 °C), V_{fb} was reduced by ~0.18 V, and continues to reduce, following further annealing. This trend was observed to become steady after annealing at 150 °C, with only a small variation (~0.01 V). The range of extracted V_{fb} values as a function of thermal annealing (0.5–0.34 V, between 100 and 150 °C) does not differ largely from other reported values [47]. Compared to the values for thermally annealed P3HT:PCBM devices reported by Guerrero et al. [47], we noticed a difference in the range of ~0.02–0.14 V higher, presumably because our devices were thermally annealed post-cathode deposition, and Al cathode was used (as opposed to Ca/Ag). Based on the cathode equilibration model involving flat-band conditions and dipole layer formation [45], we infer from our V_{fb} values that the PCBM concentration at the active layer/Al interface seems to increase with thermal annealing. This also supports the view of thermally-induced vertical segregation of PCBM molecular aggregates towards the cathode interface [12,14]. Additionally, we note that this observation is consistent with our previous optical microscopy study [13], where images of PCBM clusters on P3HT: PCBM blend film surface was observed upon thermal

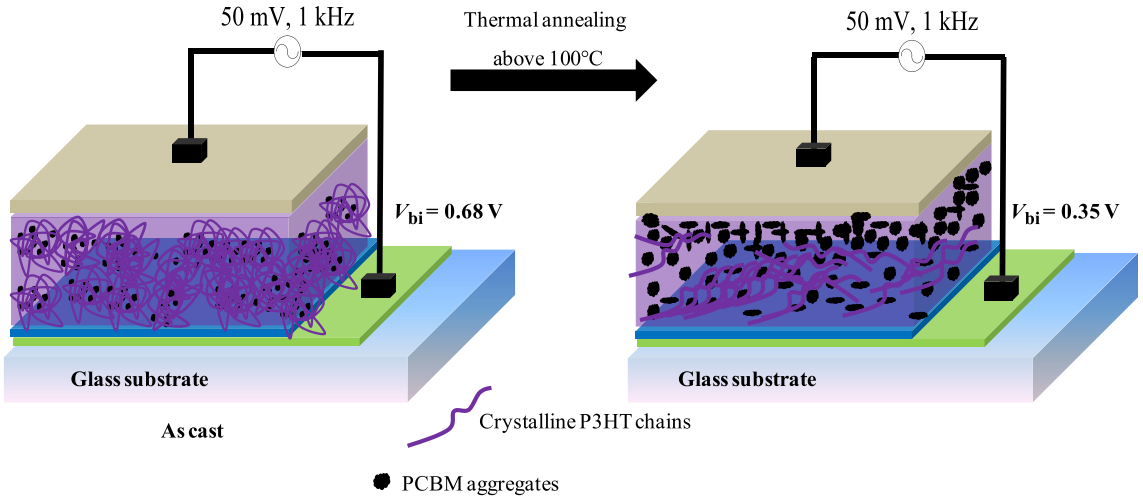

Fig. 7. A graphical schematic illustrating vertical segregation process following thermal annealing of P3HT: PCBM bulk heterojunction solar cell.

annealing. The temperature at which the cluster formation of PCBM became remarkably evident was noted at 100 °C and it is interesting that the measured V_{fb} values significantly reduces after the same 100 °C mark. Hence by performing the stepwise thermal annealing protocol, it seems that 100 °C marks a critical point in which the migration of PCBM to the top surface is initiated, after which significant nanomorphological changes begin to occur. Furthermore between 150 and 175 °C, we noticed that V_{fb} remains almost unchanged, suggesting that after annealing at 150 °C, PCBM accumulation towards the cathode interface almost reaches saturation. Especially in the cases were the top electrode restricts further migration of PCBM molecular aggregates when post-annealed. Therefore, the proposed thermally-induced vertical segregation is summarised graphically in Fig. 7. The result of such a vertical D/A profile is expected to be favourable for the efficient harvesting of charge carriers at the electrodes respectively.

4. Conclusions

Photocurrent dependence on thermal annealing in P3HT: PCBM solar cell has been previously demonstrated. It is indicative of annealing induced morphology in the blend active layer. It is also well known that via thermal annealing, optimised D/A interfaces is critical to efficient exciton dissociation. We have herein investigated the significance of charge carrier lifetimes in BHJ P3HT: PCBM solar cells. Applying ac impedance measurement analysis, the electrical properties of D/A interface was probed. Our results reveal that extending charge carrier lifetimes is significant to improving device PCEs. After annealing at the optimum temperature (150 °C), the longest charge carrier lifetime of 6.23 μs was measured, corresponding to the best device efficiency of 3.84%. Consequently, to have a system with efficient charge collection, long lived charge carriers in addition to optimised D/A interface, improved charge transport network, plays a significant role. The reduced built-in potential, V_{fb} determined from *C–V* measurement analysis as a function of thermal annealing is indicative of increased PCBM cluster concentration towards the cathode. The thermally-induced vertical segregation suggested here supports favourable contact selectivity for organic solar cells.

References

[1] P. Heremans, D. Cheyns, B.P. Rand, Strategies for increasing the efficiency of heterojunction organic solar cells: material selection and device architecture, Accounts Chem. Res. 42 (2009) 1740–1747.
[2] J. Nelson, Polymer: fullerene bulk heterojunction solar cells, Mater. Today 14 (2011) 462–470.
[3] F.C. Krebs, Fabrication and processing of polymer solar cells, A review of printing and coating techniques, Sol. Energy Mater. Sol. Cell. 93 (2009) 394–412.
[4] P. Vanlaeke, G. Vanhoyland, T. Aernouts, D. Cheyns, C. Deibel, J. Manca, P. Heremans, J. Poortmans, Polythiophene based bulk heterojunction solar cells: morphology and its implications, Thin Solid Films 511 (2006) 358–361.
[5] L. Blankenburg, K. Schultheis, H. Schache, S. Sensfuss, M. Schrödner, Reel-to-reel wet coating as an efficient up-scaling technique for the production of bulk heterojunction polymer solar cells, Sol. Energy Mater. Sol. Cell. 93 (2009) 476.
[6] R. Hegde, N. Henry, B. Whittle, H. Zang, B. Hu, J. Chen, K. Xiao, M. Dadmun, The impact of controlled solvent exposure on the morphology of, structure and function of bulk heterojunction solar cells, Sol. Energy Mater. Sol. Cell. 107 (2012) 112–124.
[7] P.P. Khlyabich, B. Burkhart, A.E. Rudenko, B.C. Thompson, Optimization and simplification of polymer-fullerene solar cells through polymer and active layer design, Polymer 54 (2013) 5267–5298.
[8] G. Li, R. Zhu, Y. Yang, Polymer solar cells, Nat. Photon. 6 (2012) 153–161.
[9] K. Kawano, J. Sakai, M. Yahiro, C. Adachi, Effect of solvent on fabrication of active layers in organic solar cells based on poly(3-hexylthiophene)and fullerene derivatives, Sol. Energy Mater. Sol. Cell. 93 (2009) 514–518.
[10] B.C. Thompson, J.M.J. Fréchet, Polymer - fullerene composite solar cells, Angew. Chem. 47 (2008) 58–77.
[11] M.T. Dang, L. Hirsch, G. Wantz, P3HT: PCBM, best seller in polymer photovoltaic research, Adv. Mater. 23 (2011) 3597–3602.
[12] A.M. Ballantyne, T.A.M. Ferenczi, M. Campoy – Quiles, T.M. Clarke, M. Maurano, K.H. Wong, W. Zhang, N. Stingelin-Stutzmann, J.-S. Kim, D.D.C. Bradley, J.R. Durrant, I. McCulloch, M. Heeney, J. Nelson, Understanding the influence of morphology on poly (3-hexylselenothiophene): PCBM solar cells, Macromolecules 43 (2010) 1169–1174.
[13] O. Oklobia, T. Sadat-Shafai, A quantitative study of the formation of PCBM clusters upon thermal annealing of P3HT/PCBM bulk Heterojunction Solar Cell, Sol. Energy Mater. Sol. Cell. 117 (2014) 1–8.
[14] M. Campoy – Quiles, T. Ferenczi, T. Agostenilli, P.G. Etchegoin, Y. Kim, T.D. Anthapoulos, P.N. Stavrinou, D.D.C. Bradley, J. Nelson, Morphology evolution via self-organisation and lateral and vertical diffusion in polymer: fullerene solar cell blends, Nat. Mater. 7 (2008) 158–164.
[15] V.D. Mihailetchi, H. Xie, B. de Boer, L.J.A. Koster, P.W.M. Blom, Charge transport and photocurrent generation in poly(3-hexylthiophene): methanofullerene bulk-heterojunction solar cells, Adv. Funct. Mater. 16 (2006) 699–708.
[16] T.M. Clarke, J.R. Durrant, Charge photogeneration in organic solar cells, Chem. Rev. 110 (2010) 6736–6767.
[17] W. Ma, C. Yang, X. Gong, K. Lee, A.J. Heeger, Thermally stable, efficient polymer solar cells with nanoscale control of the interpenetrating network morphology, Adv. Funct. Mater. 16 (2005) 1617–1622.
[18] P. Müller-Buschbaum, The active layer morphology organic solar cells probed with grazing incidence scattering techniques, Adv. Mater. 26 (2014) 7692–7709.
[19] F.C. Jamieson, E.B. Domingo, T. McCarthy-Ward, M. Heeney, N. Stingelin, J.R. Durrant, Fullerene crystallisation as a key driver of charge separation in polymer/fullerene bulk heterojunction solar cells, Chem. Sci. 3 (2012) 485–492.
[20] T. Erb, U. Zhokhavets, H. Hoppe, G. Gobsch, M. Al-Ibrahim, O. Ambacher, Fullerene crystallisation as a key driver of charge separation in polymer/fullerene bulk heterojunction solar cells, Thin Solid Films 511–512 (2006) 483–485.
[21] G. Li, V. Shrotriya, Y. Yao, Y. Yang, Investigation of annealing effects and film thickness dependence of polymer solar cells based on poly(3-hexylthiophene), J. Appl. Phys. 98 (2005) 043704 (1-5).
[22] D. Chirvase, J. Parisi, J.C. Hummelen, V. Dyakonov, Influence of nanomorphology on the photovoltaic action of polymer-fullerene composites, Nanotechnology 15 (2004) 1317–1323.
[23] T. Kuwabara, Y. Kawahara, T. Yamaguchi, K. Takahashi, Characterization of inverted-type organic solar cells with a ZnO layer as the electron collection electrode by ac impedance spectroscopy, Applied Materials & Interfaces 1 (2009) 2107–2110.
[24] F. Fabregat-Santiago, J. Bisquert, E. Palomares, L. Otero, D. Kuang, S.M. Zakeeruddin, M. Grätzel, Correlation between the photovoltaic performance

and impedance spectroscopy of dye-sensitized solar cells based on ionic liquids, J. Phys. Chem. C 111 (2007) 6550–6560.
[25] Q. Wang, J.-E. Moser, M. Grätzel, Electrochemical impedance spectroscopic analysis of dye-sensitized solar cells, J. Phys. Chem. B 109 (2005) 14945–14953.
[26] L. Han, N. Koide, Y. Chiba, T. Mitate, Modelling of an equivalent circuit for dye-sensitized solar cells, Appl. Phys. Lett. 84 (2004) 2433.
[27] M. Jaiswal, R. Menon, Equivalent circuit for an organic field-effect transistor from impedance measurement under dc bias, Appl. Phys. Lett. 88 (2006) 123504.
[28] C.-C. Hsiao, A.-E. Hsiao, S.-A. Chen, Design of hole blocking layer with electron transport channels for high performance polymer light-emitting diodes, Adv. Mater. 20 (2008) 1982–1988.
[29] W. Huang, J. Peng, L. Wang, Investigation of annealing effects on microstructure of hybrid nanocrystal-polymer solar cells by impedance spectroscopy, Synth. Met. 160 (2010) 445–449.
[30] G. Perrier, R. de Bettignies, S. Berson, N. Lemaître, S. Guillerez, Impedance spectrometry of optimized standard and inverted P3HT-PCBM organic solar cells, Sol. Energy Mater. Sol. Cell. 101 (2012) 210–216.
[31] M. Glatthaar, M. Riede, N. Keegan, K. Sylvester-Hvid, B. Zimmermann, M. Niggemann, A. Hinsch, A. Gombert, Efficiency limiting factors of organic bulk heterojunction solar cells identified by electrical impedance spectroscopy, Sol. Energy Mater. Sol. Cell. 91 (2007) 390–393.
[32] O. Oklobia, T. Sadat-Shafai, Correlation between charge carriers mobility and PCBM cluster formation and its impact on recombination process in a blend of PCBM/P3HT bulk Heterojunction solar cell, Sol. Energy Mater. Sol. Cell. 122 (2014) 158–163.
[33] B.J. Leever, C.A. Bailey, T.J. Marks, M.C. Hersam, M.F. Durstock, In situ characterisation of lifetime and morphology in operating bulk heterojunction organic photovoltaic devices by impedance spectroscopy, Advanced Energy Materials 2 (2012) 120–128.
[34] A.S. Bondarenko, G.A. Ragoisha, EIS Spectrum analyser, http://www.abc.chemistry.bsu.by/vi/analyser/, (2011).
[35] C.L. Braun, Electric field assisted dissociation of charge transfer states as a mechanism of photocarrier production, J. Chem. Phys. 80 (1984) 4157.
[36] V.D. Mihailetchi, L.J.A. Koster, J.C. Hummelen, P.W.M. Blom, Photocurrent generation in polymer-fullerene bulk heterojunctions, Phys. Rev. Lett. 93 (2004) 216601.
[37] J.R. Macdonald, Impedance Spectroscopy, John Wiley & Sons, 1987.
[38] Y. Yoon, H.J. Kim, C.–H. Cho, S. Kim, H.J. Son, M.-O. Ko, H. Kim, D.-K. Lee, J.Y. Kim, W. Lee, B.J. Kim, Carrier lifetime extension via the incorporation of robust hole/electron blocking layers in bulk heterojunction polymer solar cells, Applied Materials and Interfaces 6 (2013) 333–339.
[39] T. Ripolles-Sanchis, A. Guerrero, E. Azaceta, R. Tena-Zaera, G. Garcia-Belmonte, Electrodeposited NiO anode interfacial layers: enhancement of the charge Carrier selectivity in organic solar cells, Sol. Energy Mater. Sol. Cell. 117 (2013) 564–568.
[40] A. Guerrero, S. Loser, G. Garcia-Belmonte, C.J. Bruns, J. Smith, H. Miyauchi, S.I. Stupp, J. Bisquert, T.J. Marks, Solution-processed small molecule: fullerene bulk heterojunction solar cells: impedance spectroscopy deduced bulk and interfacial limits to fill-factors, Phys. Chem. Chem. Phys. 15 (2013) 16456–16462.
[41] A. Guerrero, N.F. Montcada, J. Ajuria, I. Etxebarria, R. Pacios, G. Garcia-Belmonte, E. Palomares, Charge Carrier transport and contact selectivity limit the operation of PTB7-based organic solar cells of varying active layer thickness, J. Mater. Chem. 1 (2013) 12345–12354.
[42] K. Ryo, Y. Yang, Vertical phase separation of conjugated polymer and fullerene bulk heterojunction films induced by high pressure carbon dioxide treatment at ambient temperature, Phys. Chem. Chem. Phys. 14 (2012) 8313–8318.
[43] S. Kim, P.K.H. Ho, C.E. Murphy, R.H. Friend, Phase Separation in Polyfluorene-based Conjugated Polymer Blends: Lateral and Vertical Analysis of Blend Spin Cast Thin Films Macromolecules vol 37, (2004), pp. 2861–2871.
[44] D.K. Susarova, P.A. Troshin, Y.L. Moskvin, S.D. Babenko, V.F. Razumov, Vertical concentration gradients in bulk heterojunction solar cells induced by differential solubility, Thin Solid Films 519 (2011) 4132–4135.
[45] A. Guerrero, L.F. Marchesi, P.P. Boix, S. Ruiz-Raga, T. Ripolles-Sancis, G. Garcia-Belmonte, J. Bisquert, How the charge-neutrality level of interface states controls energy level alignment in cathode contacts of organic bulk-heterojunction solar, ACS Nano 6 (2012) 3453–3460.
[46] H. Vázquez, F. Flores, R. Oszwaldowski, J. Ortega, R. Pérez, A. Khan, Barrier Formation at metal-organic interfaces: dipole formation and the charge neutrality level, Appl. Surf. Sci. 234 (2004) 107–112.
[47] A. Guerrero, B. Dörling, T. Ripolles-Sanchis, M. Aghamohammadi, E. Barrena, M. Campoy-Quiles, G. Garcia-Belmonte, Interplay between fullerene surface coverage and contact selectivity of cathode interfaces in organic solar cells, ACS Nano 7 (2013) 4637–4646.
[48] G. Garcia-Belmonte, A. Munar, E.M. Barea, J. Bisquert, I. Ugarte, R. Pacios, Charge Carrier lifetime of organic bulk heterojunctions analyzed by impedance spectroscopy, Org. Electron. 9 (2008) 847–851.
[49] J.V. Li, A.M. Nardes, Z. Liang, S.E. Shaheen, B.A. Gregg, D.H. Levi, Simultaneous measurement of Carrier density and mobility of organic semiconductors using capacitance techniques, Org. Electron. 12 (2011) 1879–1885.